Available online at www.sciencedirect.com
ScienceDirect
Trans. Nonferrous Met. Soc. China 23(2013) 353−360
Transactions of Nonferrous Metals Society of China
www.tnmsc.cn

High temperature deformation behavior and optimization of hot compression process parameters in TC11 titanium alloy with coarse lamellar original microstructure

Shi-qiang LU[1], Xin LI[1], Ke-lu WANG[1], Xian-juan DONG[1], M. W. FU[2]

1. School of Materials Science and Engineering, Nanchang Hangkong University, Nanchang 330063, China;
2. Department of Mechanical Engineering, The Hong Kong Polytechnic University, Kowloon, Hong Kong, China

Received 3 February 2012; accepted 2 November 2012

Abstract: The high temperature deformation behaviors of $\alpha+\beta$ type titanium alloy TC11 (Ti−6.5Al−3.5Mo−1.5Zr−0.3Si) with coarse lamellar starting microstructure were investigated based on the hot compression tests in the temperature range of 950−1100 °C and the strain rate range of 0.001−10 s^{-1}. The processing maps at different strains were then constructed based on the dynamic materials model, and the hot compression process parameters and deformation mechanism were optimized and analyzed, respectively. The results show that the processing maps exhibit two domains with a high efficiency of power dissipation and a flow instability domain with a less efficiency of power dissipation. The types of domains were characterized by convergence and divergence of the efficiency of power dissipation, respectively. The convergent domain in $\alpha+\beta$ phase field is at the temperature of 950−990 °C and the strain rate of 0.001−0.01s^{-1}, which correspond to a better hot compression process window of $\alpha+\beta$ phase field. The peak of efficiency of power dissipation in $\alpha+\beta$ phase field is at 950 °C and 0.001 s^{-1}, which correspond to the best hot compression process parameters of $\alpha+\beta$ phase field. The convergent domain in β phase field is at the temperature of 1020−1080 °C and the strain rate of 0.001−0.1 s^{-1}, which correspond to a better hot compression process window of β phase field. The peak of efficiency of power dissipation in β phase field occurs at 1050 °C over the strain rates from 0.001 s^{-1} to 0.01 s^{-1}, which correspond to the best hot compression process parameters of β phase field. The divergence domain occurs at the strain rates above 0.5 s^{-1} and in all the tested temperature range, which correspond to flow instability that is manifested as flow localization and indicated by the flow softening phenomenon in stress—strain curves. The deformation mechanisms of the optimized hot compression process windows in $\alpha+\beta$ and β phase fields are identified to be spheroidizing and dynamic recrystallizing controlled by self-diffusion mechanism, respectively. The microstructure observation of the deformed specimens in different domains matches very well with the optimized results.

Key words: titanium alloy; coarse lamellar microstructure; high temperature deformation behavior; processing map; hot compression process; parameter optimization

1 Introduction

TC11 is an $\alpha+\beta$ type titanium alloy widely used for applications in the components of aircraft engine. This alloy has a nominal composition of Ti−6.5Al−3.5Mo−1.5Zr−0.3Si (mass fraction, %) with the β transus temperature of about 1008 °C. The properties of titanium alloy are mainly dependent on its microstructures, which are related to chemical composition, hot working history and heat treatment process [1]. During high temperature deformation, the shape and the microstructure are changed simultaneously at different temperatures and strain rates [2,3]. Since different microstructures have different properties [3], thus, the microstructure should be strictly controlled during deformation in such a way to obtain the needed properties of forgings. To strictly control the microstructure, the forging process parameters must be controlled strictly as the microstructure of the titanium alloy is very sensitive to the deformation temperature and strain rate [4]. The irrational forging process windows could result in the occurrence of various metallurgical defects such as adiabatic shear band, flow localization, dynamic strain aging, and the reduction of mechanical properties of the forgings.

Foundation item: Project (51005112) supported by the National Natural Science Foundation of China; Project (2010ZF56019) supported by the Aviation Science Foundation of China; Project (GJJ11156) supported by the Education Commission of Jiangxi Province, China; Project (GF200901008) supported by the Open Fund of National Defense Key Disciplines Laboratory of Light Alloy Processing Science and Technology, China

Corresponding author: Shi-qiang LU; Tel/Fax: +86-791-3863039; E-mail: niatlusq@126.com

DOI: 10.1016/S1003-6326(13)62469-3

Processing map technique is very useful to correlate hot working process parameters with microstructure evolutions. The theory of processing map is based on the dynamic materials model and was developed by PRASAD et al [5−7]. At present, the processing map is widely used to predict flow instability [8−10], optimize process parameters [11,12] and control microstructure of the hot working components for many materials [13,14]. It is an effective approach for design and optimization of hot working process parameters. From a thermodynamics viewpoint, the workpiece in hot working process may be viewed as a closed system, where the total absorbed power (p) from equipment is dissipated through the temperature rise and microstructure change of the workpiece. The dissipated powers caused by the temperature rise and microstructure change are called G content and J co-content, respectively. The strain rate sensitivity of flow stress (m) decides the partition of the total power between G and J. For an ideal plastic flow (m=1), J reaches its maximum $J_{max}=p/2$. Thus, a dimensionless parameter called the efficiency of power dissipation (η) is derived by comparing the non-linear power dissipation (m<1) occurring instantaneously in the workpiece with that of a liner dissipater (m=1) and defined as [15]

$$\eta=\frac{J}{J_{\max}}=\frac{2m}{m+1} \tag{1}$$

The variation of η with temperature and strain rate constitutes a power dissipation map. In order to identify the regime of flow instability, a continuum instability criterion is developed according to the extremum principle of irreversible thermodynamics as applied to large plastic flow and given by [16]

$$\xi(\dot{\varepsilon})=\frac{\partial \ln(\frac{m}{m+1})}{\partial \ln\dot{\varepsilon}}+m<0 \tag{2}$$

The variation of $\xi(\dot{\varepsilon})$ with temperature and strain rate constitutes an instability map, which is superimposed on a power dissipation map to develop a processing map. In a processing map, there are some domains where different microstructural mechanisms operate, and flow instabilities are predicted to occur when $\xi(\dot{\varepsilon})$ becomes negative.

The original microstructure with coarse lamellar is one of the common microstructures prior to forging apart from the equiaxed original microstructure. The forging process optimization for titanium alloy TC11 with equiaxed original microstructure has already been investigated [17], but there is no literature found so far for the optimization of forging process parameters for the alloy with coarse lamellar original microstructure. To optimize the forging process parameters and control the microstructure of the alloy with coarse lamellar starting microstructure, the high temperature deformation behaviors and deformation mechanisms are investigated, and the optimal hot compression process window is also determined in this work. The research provides the basis and fundamental for production of the alloy forgings with high quality and good mechanical properties.

2 Experimental

The as-received TC11 alloy is a cylindrical billet with the diameter of 150 mm. The billet was soaked at the temperature of 1040 °C for 30 min and furnace-cooled to room temperature in such a way that the coarse lamellar original microstructure, as shown in Fig. 1, was obtained. The microstructure consists of equiaxed prior β grains containing a transformed structure of colony α. The prior β grain size is approximately 642 μm, and the mean thickness of α lamella is about 2.4 μm. The as-received billet was machined into the cylindrical compression specimens with the dimensions of 8 mm in diameter and 12 mm in height. The isothermally constant strain rate compression tests were conducted in the temperature range of 950−1100 °C with the interval of 50 °C and the strain rate range of 0.001−10 s^{-1} at an interval of an order magnitude by using a THERMECMASTOR-Z hot working simulator. The specimens were heated at a rate of 10 °C/s up to the deformation temperature and soaked for 210 s to make the specimen temperature homogeneous. In addition, the temperature of the

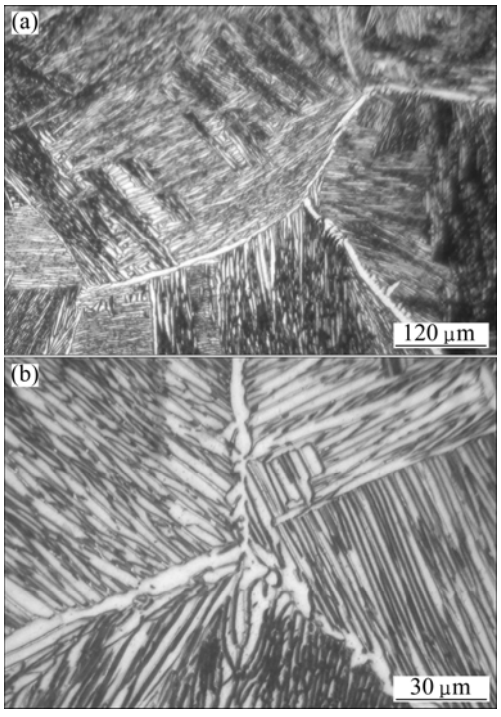

Fig. 1 Original microstructures of as-received TC11 alloy: (a) Lower magnification; (b) Higher magnification

specimen was monitored by using a platinum-rhodium thermocouple welded at the middle of specimen and the isothermal condition was maintained within ±1 °C.

All the specimens were compressed up to a true strain of 0.7, which is equivalent to the height reduction of 50%. The specimens were then helium gas-jet cooled immediately to room temperature at a rate of about 40 °C/s to retain the deformed microstructure at high temperatures. The deformed specimens were sectioned into two parts along the compression direction and the cut surfaces were polished and etched in a solution of 4% HF, 16% HNO_3, and 80% H_2O (volume fraction). The microstructure observation was then conducted by using optical microscope (OM).

3 Results and discussion

3.1 Stress—strain curve

The stress—strain curves of the alloy obtained at different strain rates and temperatures are shown in Fig. 2. It is found from Fig. 2 that the stress—strain curves at the temperatures of 1000, 1050 and 1100 °C, show similar characteristics due to the fact that these temperatures are in β phase field or slightly lower than β transus temperature (1008 °C) and the deformation is mainly controlled by β phase. At these temperatures, the curves exhibit a peak stress at a relatively low strain followed by the moderate flow softening at the strain rate of 0.1 s^{-1} and above. The curves have a steady state at the strain rate below 0.1 s^{-1}. But at the temperature of 950 °C, all the curves, except for the case of 0.001 s^{-1}, exhibit flow softening after a peak stress. The microstructure change and/or the deformation heating are responsible for the flow softening [18]. The flow softening at low strain rates or high temperatures is mainly caused by the microstructure change. At high strain rates or low temperatures, it is mainly attributable to the deformation heating due to the low thermal conductivity of the titanium alloy and the short deformation time. The steady state flow behavior at lower strain rates means that the dynamic softening balances to work hardening. The mechanisms for dynamic softening in $\alpha+\beta$ field and β field could be spheroidization and dynamic recrystallization, respectively [19]. The peak flow stresses at all tested temperatures are observed to increase with increasing strain rates and decreasing temperature. In addition, it is found that the higher the strain rate, the higher the increasing rate of flow stress. Therefore, the flow stress is significantly affected by the deformation temperature and strain rate. The above results indicate that the TC11 alloy with coarse lamellar original microstructure has a

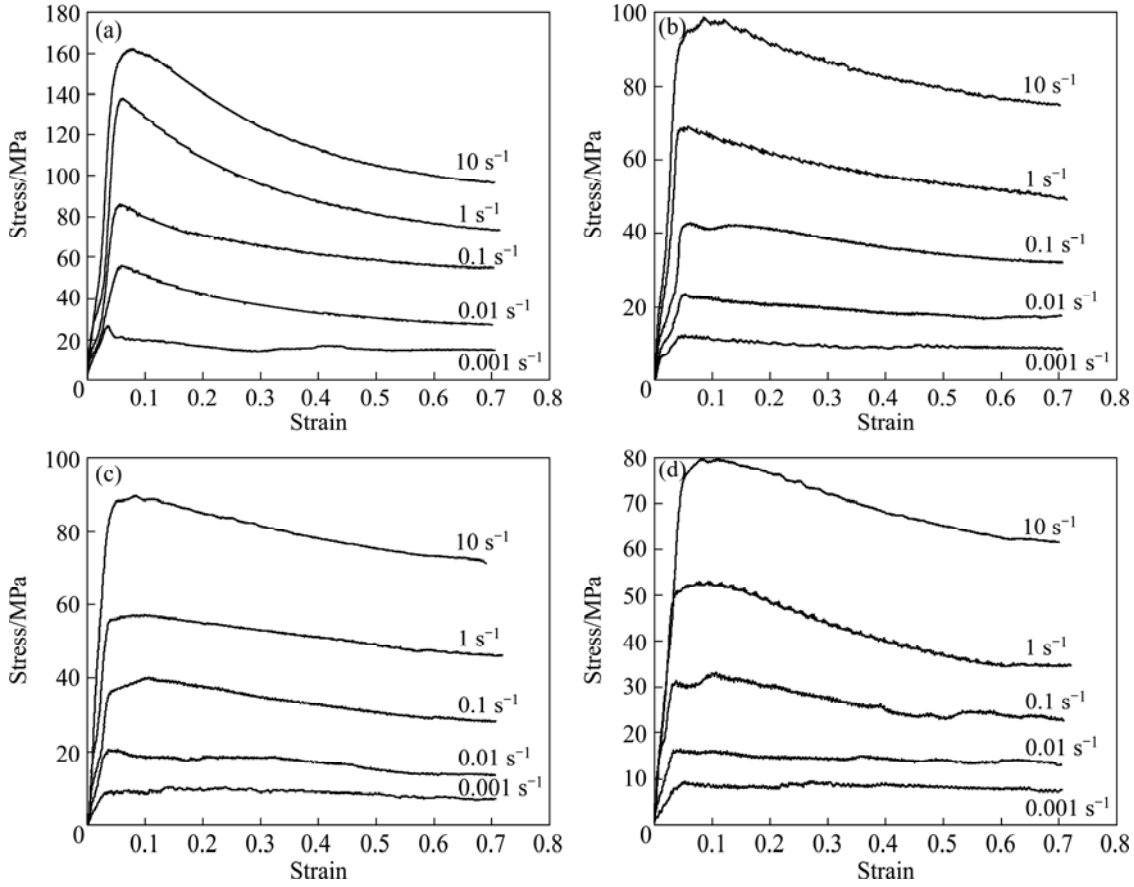

Fig. 2 Stress—strain curves of alloy at different strain rates and temperatures: (a) 950 °C; (b) 1000 °C; (c) 1050 °C; (d) 1100 °C

poor workability and the deformation should be taken under low strain rates.

3.2 Processing map

In order to obtain many more flow stresses and facilitate the calculation of η and $\xi(\dot{\varepsilon})$ values under different temperatures, strain rates and strains, the experimental data of isothermally constant strain rate compression are first interpolated by the cubic spline; and then the method of the least square polynomial fitting is used for data processing, finally the processing maps at the strains of 0.2 and 0.6 are constructed, as shown in Fig. 3. In Fig. 3, the contour numbers represent the values of η and the shaded regions correspond to flow instability where the values of $\xi(\dot{\varepsilon})$ are negative. It can be seen that there are two convergent domains with high value of η and a divergence domain with a lower value of η in the processing maps. The convergent domain in which the value of η is getting bigger and bigger towards the centre of the domain represents the better hot compression process window. The divergence domain in which the value of η is getting smaller and smaller towards the centre of the domain represents the flow instability window. The two convergent domains

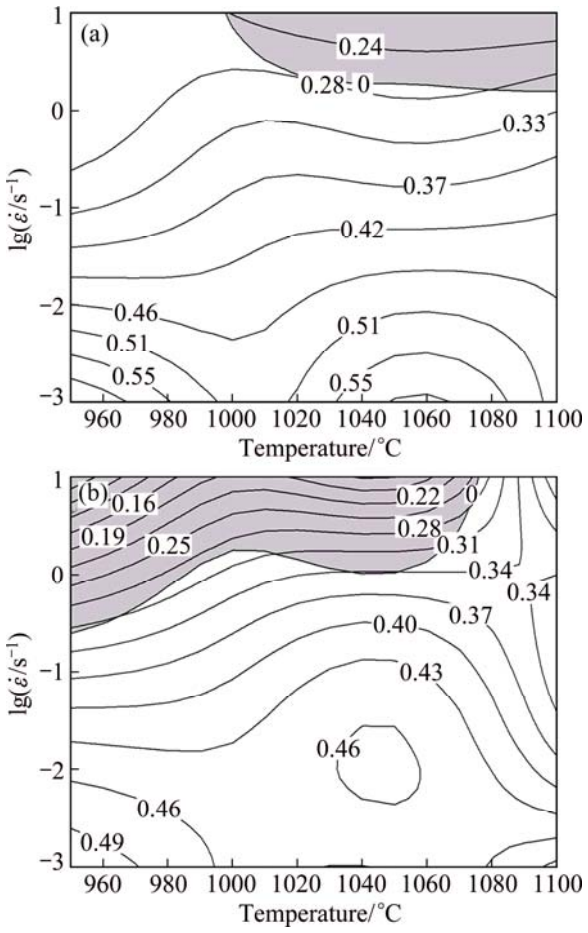

Fig. 3 Processing maps of alloy at strains of 0.2 (a) and 0.6 (b)

are in α+β (at 950−990 °C) and β fields (at 1020−1080 °C), respectively. In addition, it is found that the strain affects the location and area of the convergent domain and the flow instability domain to a certain extent.

The convergent domain in α+β phase field has an appreciable trend extending to lower temperatures and strain rates with the increase of strain, moreover, η may reach a higher value with decreasing temperature and strain rate, as shown in Fig. 3. This domain is about in the temperature range of 950−990 °C and strain rate range of 0.001−0.01 s^{-1}, which represents the better hot compression process window due to its high η value and convergent characteristics. The η value of the domain is greater than 0.46 and its peak value of 0.55−0.65 is at 950 °C and 0.001 s^{-1}, which are the best hot compression process parameter. The η value as high as 0.55−0.65 indicates that the deformation mechanism in this domain could be dynamic recrystallization or superplasticity or spheroidization [15,19]. In general, the sliding of grain boundaries will be involved during superplastic deformation [20], which needs fine and equiaxed grains to provide adequate sliding interfaces and needs two phases to prevent mutual growth. But for the studied TC11 alloy, α phase is coarse lamellar, the superplasticity can thus be eliminated. In this domain, the typical micrographs of the specimens deformed at 900 °C and the strain rates of 0.01 s^{-1} and 0.001 s^{-1} are shown in Figs. 4(a) and (b) respectively, it is obviously seen that spheroidizing of α lamellae takes place. The volume fraction of the spheroidized α phase at 0.001 s^{-1} is more than that at 0.01 s^{-1}, which suggests that the

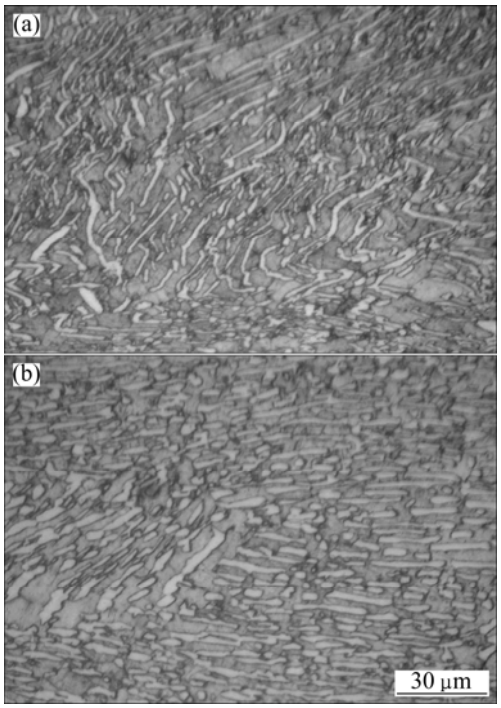

Fig. 4 Microstructures of alloy deformed at 950 °C under different strain rates: (a) 0.01 s^{-1}; (b) 0.001 s^{-1}

spheroidization nucleation depends on the strain rate. This result is agreement with that studied by LI et al [21]. Furthermore, the size of the spheroidized α phase increases with decreasing strain rate. This is because there is more time for the spheroidization of α lamellae and the growth of spheroidized α phase in low strain rate deformation process. SESHACHARYULU et al [19,22] investigated the spheroidization process of α lamellae in Ti−6Al−4V alloy and proposed that the spheroidization process may be regarded as a type of dynamic recrystallization since it involves two competitive processes, i.e., rate of nucleation and rate of migration. The spheroidizing deformation mechanism and the spheroidized microstructure in α+β phase field are favorable for workability and mechanical properties of the alloy, respectively, which indicates that the above optimized forging process window based on the processing map is right and reasonable.

The convergent domain in β phase field obviously shifts toward higher strain rates with increasing strain, as shown in Fig. 3. This domain is about in the temperature range of 1020−1080 °C and strain rate range of 0.001−0.1 s^{-1}, which presents the better hot compression process window. The η value of the domain is greater than 0.42 and its peak value of 0.52−0.61 occurs at a temperature of 1050 °C and a strain rate range of 0.001−0.01 s^{-1}, which correspond to the best hot compression process parameters. In this domain, the typical micrographs of the specimens deformed at 1050 °C and the rates of 0.1, 0.01 and 0.001 s^{-1} are shown in Fig. 5. In Fig. 5, the dynamic recrystallizing characteristics of β can be obviously observed. It can also be seen that the dynamic recrystallization only took place partly at 0.1 s^{-1} (Fig. 5(a)), while fully happened at 0.01 and 0.001 s^{-1} (Figs. 5(b) and (c)). The average dynamic recrystallized β grain size increases with decreasing strain rates. The average dynamic recrystallized β grain sizes measured by image analysis Software installed in the optical microscope system are about 24.9, 36.5 and 78.9 μm at 0.1, 0.01 and 0.001 s^{-1}, respectively. Since the fine grain is helpful for obtaining excellent strength and good plasticity, thus, the strain rate of 0.01 s^{-1} is preferable for hot compression of the alloy in β phase field.

The dynamic recrystallizing deformation mechanism and dynamic recrystallized microstructure in β phase field are desirable for workability and mechanical properties respectively, which mean that the above optimized hot compression process window based on the processing map is right and reasonable.

The flow instability domain (i.e., the divergence domain) predicted by the instability criterion (Eq. (2)) has a trend shifting to lower strain rates and temperatures with increasing strain, as shown in Fig. 3. The process

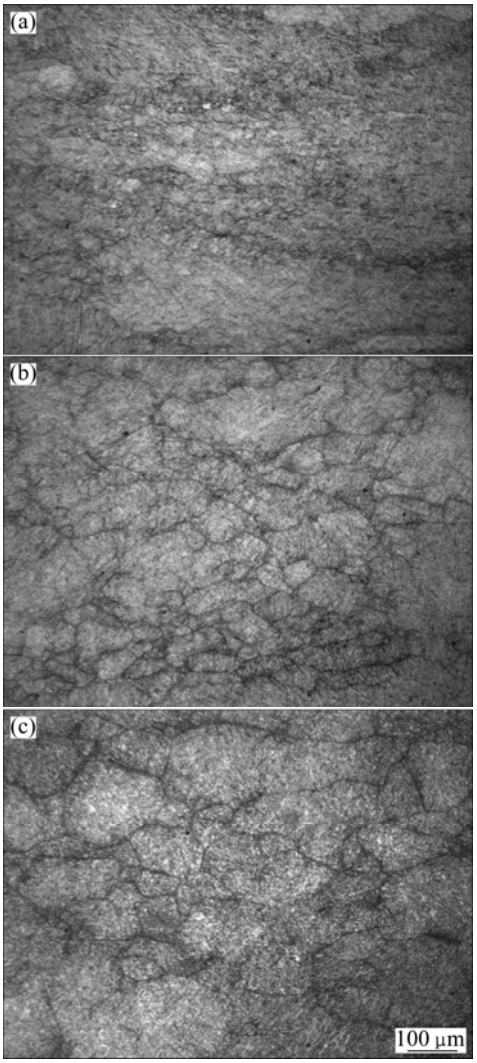

Fig. 5 Microstructures of alloy deformed at 1050 °C under different strain rates: (a) 0.1 s^{-1}; (b) 0.01 s^{-1}; (c) 0.001 s^{-1}

window of this domain is at the high strain rate of above 0.5 s^{-1} and whole investigated temperatures. The η value in this domain is less than 0.3, furthermore, the variation of η values is divergent, which are typical characteristic of the flow instability domain. The prediction of flow instability domain based on the processing map is validated via the observation of the manifestation of flow instability in the deformed specimen. The microstructures of the specimens deformed at the same strain rate of 10 s^{-1} and temperatures of 950 °C and 1050 °C are shown in Figs. 6(a) and (b), respectively. These microstructures exhibit flow localization at angles of 20°−40° to the compression direction. The generation of flow localization mainly attributes to the short deformation time and low thermal conductivity of the alloy. The flow localization is also indicated by the flow softening in stress—strain curves as discussed above.

The flow localizing is a deleterious deformation mechanism for workability, and the generated

microstructure is also not good for mechanical properties, therefore, the flow instability process window must be avoided in the practical hot compression.

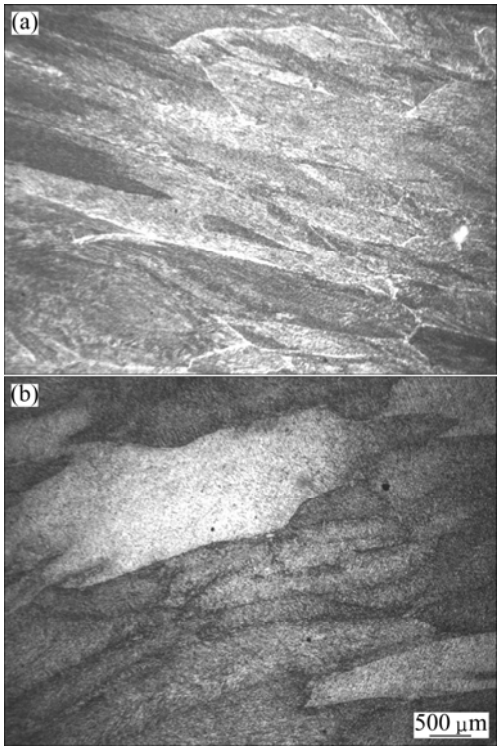

Fig. 6 Microstructures of alloy deformed at 10 s^{-1} under different temperatures: (a) 950 °C; (b) 1050 °C

3.3 Kinetic analysis

In order to assist in identifying the operative microstructural mechanisms during the dynamic recrystallization process of β phase, the value of activation energy for the alloy is calculated based on the following kinetic rate equation [23]:

$$\dot{\varepsilon}\exp\left(\frac{Q}{RT}\right)=A\sigma^{n} \tag{3}$$

where $\dot{\varepsilon}$ is the strain rate; Q is the activation energy; R is the gas constant; T is the temperature; A is a constant; σ is the flow stress and n is the stress exponent. Thus, the activation energy Q can be determined by using the following expression:

$$Q=Rn\left[\frac{\partial\ln\sigma}{\partial(1/T)}\right]_{\varepsilon} \tag{4}$$

where n can be calculated by

$$n=\frac{\partial\ln\dot{\varepsilon}}{\partial\ln\sigma}\Big|_{T} \tag{5}$$

The plots of $\ln\dot{\varepsilon}$ versus $\ln\sigma$ and $\ln\sigma$ versus $1/T$ at strains of 0.2 and 0.6 in the temperature range of 1000−1100 °C and the strain rate range of 0.001−10 s^{-1} are shown in Figs. 7 and 8, respectively. The slope values of the lines in Figs. 7(a) and 8(a) are the stress

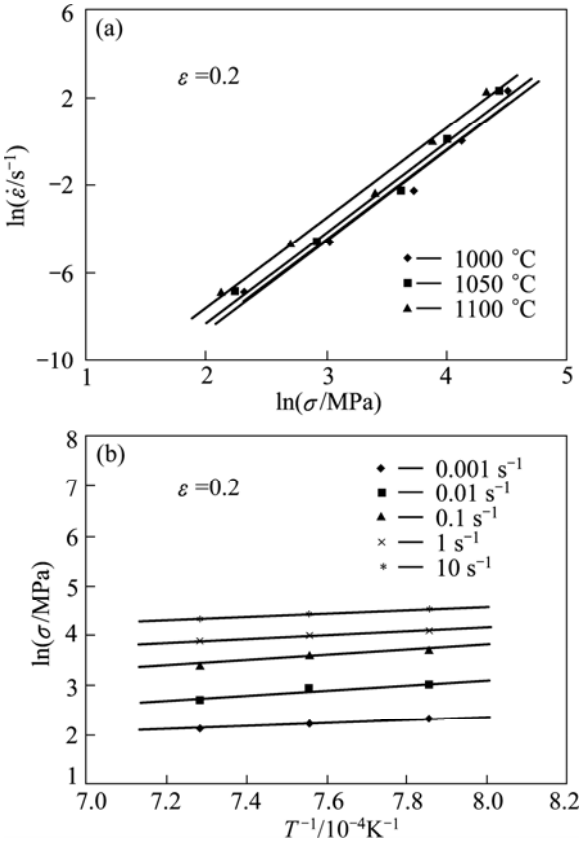

Fig. 7 Plots of $\ln\dot{\varepsilon}$ vs $\ln\sigma$ (a) and $\ln\sigma$ vs $1/T$ (b) at strain of 0.2

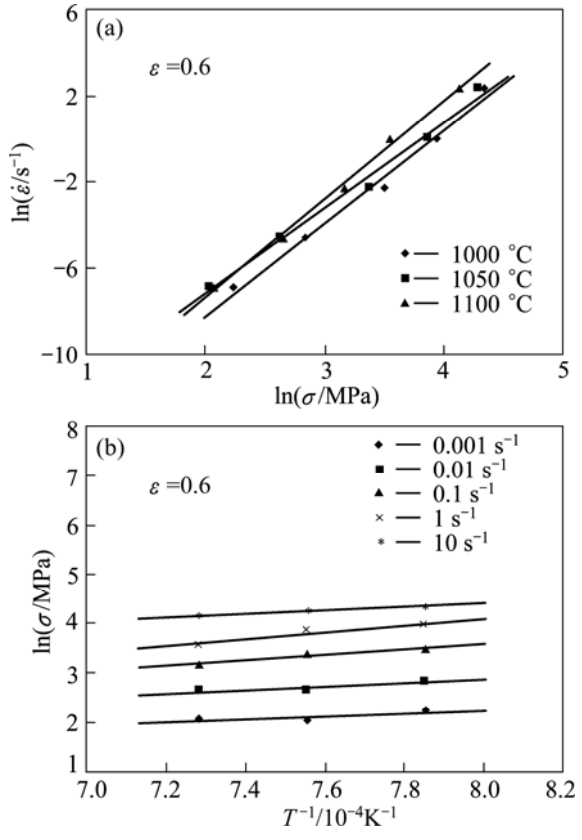

Fig. 8 Plots of $\ln\dot{\varepsilon}$ vs $\ln\sigma$ (a) and $\ln\sigma$ vs $1/T$ (b) at strain of 0.6

exponent n at strains of 0.2 and 0.6, and the values of n at these two stains are 4.1 and 4.3 by calculation, respectively. According to Figs. 7 and 8, the activation energies of 157.1 and 147.7 kJ/mol at strains of 0.2 and 0.6 are calculated. The approximately equal activation energies indicate that the deformation mechanisms at these two strains are the same. The calculated activation energies are very close to that of the self-diffusion in β-Ti (153 kJ/mol) [24], which suggests that the dynamic recrystallization of β phase is diffusion controlled. Similar conclusion was also found in commercial grade Ti−6Al−4V with lamellar starting structure by SESHACHARYULU et al [19].

4 Conclusions

1) TC11 alloy with coarse lamellar original microstructure has a poor workability. The two domains with high and convergent efficiency of power dissipation and a flow instability domain with less and divergent efficiency of power dissipation are predicted based on the processing maps of the alloy. The location and the area of these domains are influenced by strain to a certain extent, namely, the convergent domain in $\alpha+\beta$ phase field slightly extends to lower temperatures and strain rates, while in β phase field, it obviously shifts toward higher strain rates, the flow instability domain shifts to lower strain rates and temperatures, with increasing strain.

2) The convergent domain in $\alpha+\beta$ phase field occurs at the temperatures of 950−990 °C and the strain rates of 0.001−0.01 s^{-1}, and the peak of efficiency of power dissipation presents at 950 °C and 0.001 s^{-1}, which correspond to the better hot compression process window and the best hot compression process parameters, respectively. The good workability due to occurrence of spheroidizing deformation mechanism and good mechanical properties due to formation of spheroidized microstructure can be obtained when the optimal hot compression process is adopted.

3) The convergent domain in β phase field occurs in the temperature range of 1020−1080 °C and the strain rate range of 0.001−0.1 s^{-1}, and the peak of efficiency of power dissipation occurs at 1050 °C and the strain rate range of 0.001−0.01 s^{-1}, which correspond to the better hot compression process window and the best hot compression process parameters, respectively. The activation energy for hot deformation in β phase field has been calculated to be 147.7−157.1 kJ/mol, which means that the dynamic recrystallization of β phase is diffusion controlled. The good workability because of occurrence of dynamic recrystallizing deformation mechanism and good mechanical properties due to formation of dynamic recrystallized microstructure can be achieved when the optimal hot compression process is adopted.

4) The flow instability domain with less and divergent efficiency of power dissipation emerges at all experimental temperatures and the strain rates higher than 0.5 s^{-1}. The flow instability process window must be avoided in practical hot compression of the alloy because of manifestation of flow localization which is deleterious for both workability and mechanical properties.

References

[1] DING R, GUO Z X, WILSON A. Microstructural evolution of a Ti−6Al−4V alloy during thermomechanical processing [J]. Materials Science and Engineering A, 2002, 327: 233−245.

[2] WANGJARA P, JAHAZI M, MONAJATI H, YUE S. Influence of thermomechanical processing on microstructural evolution in near-α alloy IMI834 [J]. Materials Science and Engineering A, 2006, 416: 300−311.

[3] MA F C, LU W J, QING J N, ZHANG D. Microstructure evolution of near-α titanium alloys during thermomechanical processing [J]. Materials Science and Engineering A, 2006, 416: 59−65.

[4] ABBASI S M, MOMENI A. Effect of hot working and post-deformation heat treatment on microstructure and tensile properties of Ti−6Al−4V alloy [J]. Transactions of Nonferrous Metals Society of China, 2011, 21: 1728−1734.

[5] PRASAD Y V R K, GEGEL H L, DORAIVELU S M, MALAS J C, MORGAN J T, LARK K A, BARKER D R. Modeling of dynamic material behavior in hot deformation: forging of Ti−6242 [J]. Metallurgical Transactions A, 1984, 15(10): 1883−1892.

[6] PRASAD Y V R K. Author's reply: Dynamic materials model: basis and principles [J]. Metallurgical and Materials Transactions A, 1996, 27: 235−236.

[7] PRASAD Y V R K, SESHACHARYULU T. Modeling of hot deformation for microstructural control [J]. International Materials Reviews, 1998, 43(6): 243−258.

[8] SELVAN S A, RAMANATHAN S. Hot workability of as-cast and extruded ZE41A magnesium alloy using processing maps [J]. Transactions of Nonferrous Metals Society of China, 2011, 21: 257−264.

[9] VENUGOPAL S, VENUGOPAL P, MANNAN S L. Optimization of cold and warm workability of commercially pure titanium using dynamic materials model (DMM) instability maps [J]. Journal of Materials Processing Technology, 2008, 202: 201−215.

[10] NIU Yong, HOU Hong-liang, LI Miao-quan, LI Zhi-qiang. High temperature deformation behavior of a near alpha Ti600 titanium alloy [J]. Materials Science and Engineering A, 2008, 492: 24−28.

[11] SUN Y, ZENG W D, ZHAO Y Q, ZHANG X M, MA X, HAN Y F. Constructing processing map of Ti40 alloy using artificial neural network [J]. Transactions of Nonferrous Metals Society of China, 2011, 21: 159−165.

[12] SIVAPRASAD P V, VENUGOPAL S, DAVIES C H J, PRASAD Y V R K. Identification of optimum process parameters for hot extrusion using finite element simulation and processing maps [J]. Modelling and Simulation in Materials Science and Engineering, 2004, 12: 285−291.

[13] PLLETTI C, DEGISCHER H P, KREMMER S, MARKETZ W. Processing maps of Ti662 unreinforced and reinforced with TiC particles according to dynamic models [J]. Materials Science and Engineering A, 2008, 486: 127−137.

[14] RAMANATHAN S, KARTHIKEYAN R, GANASEN G. Development of processing maps for 2124Al/SiC_p composites [J]. Materials Science and Engineering A, 2006, 441: 321−325.
[15] SAMANTARAY D, MANDAL S, BHADURI A K. Optimization of hot working parameters for thermo-mechanical processing of modified 9Cr-1Mo (P91) steel employing dynamic materials model [J]. Materials Science and Engineering A, 2011, 528: 5204−5211.
[16] KRISHAN V G, PRASAD Y V R K, BIRLA N C, RAO G S. Processing map for the hot working of near-α titanium alloy 685 [J]. Journal of Materials Processing Technology, 1997, 71: 377−383.
[17] WANG Ke-lu, LU Shi-qiang, FU M W, LI Xin, DONG Xian-juan. Optimization of *β*/near-*β* forging process parameters of Ti−6.5Al−3.5Mo−1.5Zr−0.3Si by using process maps [J]. Materials Characterization, 2009, 60: 492−498.
[18] SEMIATIN S L, SEETHARAMAN V, WEISS I. Flow behavior and globularization kinetics during hot working of Ti−6Al−4V with a colony alpha microstructure [J]. Materials Science and Engineering A, 1999, 263: 257−271.
[19] SESHACHARYULU T, MEDEIROS S C, FRAZIER W G, PRASAD Y V R K. Microstructural mechanisms during hot working of commercial grade Ti−6Al−4V with lamellar starting structure[J]. Materials Science and Engineering A, 2002, 325: 112−125.
[20] KIM J S, KIM J H, LEE Y T, PARK C G, LEE C S. Microstructural analysis on boundary sliding and its accommodation mode during superplastic deformation of Ti–6Al–4V alloy [J]. Materials Science and Engineering A, 1999, 263: 272−280.
[21] LI A B, HUANG L J, MENG Q Y, GENG L, CUI X P. Hot working of Ti−6Al−3Mo−2Zr−0.3Si alloy with lamellar *α*+*β* starting structure using processing map [J]. Materials and Design, 2009, 30: 1625−1631.
[22] SESHACHARYULU T, MEDEIROS S C, MORGAN J T, MALAS J C, FRAZIER W G, PRASAD Y V R K. Hot deformation mechanisms in ELI grade Ti−6Al−4V[J]. Scripta Materialia, 1999, 41(3): 283−288.
[23] SELLARS C M, MCTEGART W J. On the mechanism of hot deformation [J]. Acta Metallurgica, 1966, 14: 1136−1138.
[24] DYMENT F, LIBANATI C M. Self-diffusion of Ti, Zr, and Hf in their HCP phases, and diffusion of in HCP Zr [J]. Journal of Materials Science, 1968, 3: 349−359.

粗层片原始组织的 TC11 钛合金热变形行为及其热压缩工艺参数优化

鲁世强[1]，李 鑫[1]，王克鲁[1]，董显娟[1]，傅铭旺[2]

1. 南昌航空大学 材料科学与工程学院，南昌 330063；
2. 香港理工大学 机械工程系，香港九龙

摘 要：基于粗层片原始组织的 *α*+*β* 型 TC11 钛合金的热压缩实验，研究了该合金在 950~1100 °C、0.001~10 s^{-1} 条件下的热变形行为；依据动态材料模型构建了不同应变下的加工图，并对热压缩工艺参数和变形机制分别进行优化和分析。结果表明，加工图中存在 2 个功率耗散效率较高区和 1 个功率耗散效率较低的流变失稳区。这些区域的功率耗散效率呈现出收敛或发散的特征。在 *α*+*β* 两相区，功率耗散效率收敛区位于 950~990 °C、0.001~0.01 s^{-1} 范围，其峰值功率耗散效率出现在 950 °C、0.001 s^{-1}，前者和后者分别为 *α*+*β* 两相区较佳和最佳的热压缩工艺窗口；在 *β* 单相区，功率耗散效率收敛区位于 1020~1080 °C、0.001~0.1 s^{-1} 范围，其峰值功率耗散效率出现在 1050 °C、0.001~0.01 s^{-1}，前者和后者分别为 *β* 相区的较佳和最佳的热压缩工艺窗口。功率耗散效率发散区位于应变速率大于 0.5 s^{-1} 的范围内，其对应的流动失稳机制为局部流动，此时流变应力呈现出流变软化现象。在 *α*+*β* 两相区和 *β* 单相区优化工艺窗口内的变形机制分别为动态球化和自扩散控制的动态再结晶。优化结果与变形组织观察结果吻合良好。

关键词：TC11 钛合金；粗层片组织；高温变形行为；加工图；热压缩工艺；参数优化

(Edited by Xiang-qun LI)